System With RF Power Delivery Capabilities for Active Safety Enhancement in Industrial Vehicles Using Interchangeable Implements

Alessandro Bertacchini, *Member, IEEE*, Giacomantonio Napoletano, Stefano Scorcioni, Luca Larcher, *Member, IEEE*, and Paolo Pavan, *Senior Member, IEEE*

***Abstract*—In this paper, an active system for safety enhancement in industrial and off-highway vehicles using interchangeable implements is presented. The system, applied to the real case study of automatic identification of implements connected to a telehandler, is developed by adopting a hardware–software codesign approach. It is comprised of two devices: the Illuminator-Gateway Device (IGD) and the End Device (ED). Differently from other similar solutions, the system embeds a complete radio frequency (RF) power delivery system that is compliant with the regulations in force in Europe and in North America to extend the battery lifetime of the ED. In particular, the IGD, positioned on the free end of the telescopic arm of the telehandler, supplies the RF energy required for the operations of the ED and acts as a gateway sending the data received from the ED to the other Electronic Control Units (ECUs) of the vehicle. The ED, instead, is mounted on the connected implement, collects the RF energy delivered by the IGD, and wirelessly sends the unique identifier, the key parameters, and the calculated effective working time of the implement. This information can be used by the main ECU of the vehicle for safety-related purposes and programmed maintenance. Experimental results show that the implemented RF power delivery system is able to gather up to 63% of the power required by the ED when it is on duty, thus significantly extending its battery lifetime.**

***Index Terms*—Active safety, HW/SW codesign, low power electronics, RF energy harvesting, RF power delivery.**

I. Introduction

A growing number of industrial and off-highway vehicles demand an improvement of their safety systems. Differently from the automotive, where huge efforts have been spent to introduce advanced electronic systems for active pre-crash safety of the passengers, the efforts in industrial and off-highway vehicles as well as in earthmoving machineries have been mostly focused in the introduction of passive safety systems (e.g., roll-bars). While, the development of dedicated electronic devices for active and pre-crash safety in this environments has collected lacking in interest. Nowadays, the introduction of new enabling technologies allowed boosting the research activities on these topics. Among others, wireless sensor nodes and energy harvesting devices are the two technologies that allowed overcoming some of the most limiting factors in the extensive use of electronic systems for active safety applications in fields different from automotive.

In particular, most of the implements used by industrial and off-highway vehicles, earthmoving machineries and tractors have no electronic devices on board, therefore they do not have any possibility to communicate with the main vehicle. From a safety point of view, the absence of electronic devices on the implements avoids to have any input data warning about the presence and the working conditions of a connected implement. A conceptually very simple function like the automatic identification of the connected implement allows avoiding dangerous operations or dangerous working conditions related to the execution of a specific task by means of implements not fully compatibles with the machinery on which they are mounted. At the same time, it allows improving safety functions already available for industrial and off-highway vehicles or it allows implementing new ones. For example, if the main vehicle is a telehandler (like in the case study considered in this paper), the stability control algorithms running on its main ECU can be optimized by updating their input parameters in real-time accordingly with the specific characteristics of the connected implement. Indeed, up today, the implemented algorithms neglected the effects of variations in the dynamics of the whole machinery occurring when an implement is connected to the vehicle. This occurs because the ECUs on which the algorithms run do not know if an implement is connected to the vehicle and, if yes, they do not know which kind of implement is the connected one. To bypass this limitation keeping a high degree of safety, the algorithms consider always the worst working condition. This generates two different kind of problems: i) the load chart imposed by the main ECU can limit the right execution of the task; ii) the operator is encouraged to ignore the safety warnings because the suggested load chart is too much conservative. Consequently, he forces a not proper use of the implement by means of manual settings and/or taking shortcuts to save time. The result is that the safety of both machinery and operator is demanded only to the experience of the operator. The behavior and the safety conditions of the whole machinery, instead, change drastically if there is a connected implement

Manuscript received June 16, 2015; revised November 6, 2015 and February 24, 2016; accepted April 6, 2016. The Associate Editor for this paper was F. Qu.

A. Bertacchini, S. Scorcioni, and L. Larcher are with the Dipartimento di Scienze e Metodi dell'Ingegneria (DISMI), Università di Modena e Reggio Emilia, 42122 Reggio Emilia, Italy (e-mail: alessandro.bertacchini@unimore.it; scorcioni.stefano@gmail.com; luca.larcher@unimore.it).

G. Napoletano and P. Pavan are with the Dipartimento di Ingegneria "Enzo Ferrari" (DIEF), Università di Modena e Reggio Emilia, 42125 Modena, Italy (e-mail: g.antonio.napoletano@gmail.com; paolo.pavan@unimore.it).

Color versions of one or more of the figures in this paper are available online at http://ieeexplore.ieee.org.

Digital Object Identifier 10.1109/TITS.2016.2554605

or not, as well as they change also depending on the specific implement in use. For these reasons, information coming directly from the connected implement can contribute to an automatic reconfiguration of both control stability algorithms and safety limits of the whole machinery, according with the implement in use and the task that has to be executed (forcing an automatic derating of the machine operating limits if a not fully compatible implement is in use). Moreover, the identification of the connected implement together with its key parameters can enable additional safety functions. For example, combining the data of the connected implement with the data coming from other sensors already available on the vehicles, the dedicated ECU can update in real time its input parameters in order to use the optimal load chart for every working condition and for every implement.

Consequently, the use of wireless devices offers two huge benefits for all the vehicles using interchangeable implements: i) it allows using smart devices where traditional wired sensors cannot be used due to specific constraints (e.g., physical dimensions, placement in location dangerous or inaccessible, etc. . .); ii) it gives the possibility to exchange data between implement and main vehicle.

RFID technology has been the first technology investigated by the researchers of both academia and industry. But it presents still some limits in terms of sensitivity and maximum transmission range of the tags (passive RFID) or duration of the battery of the tags which is not comparable with the lifetime of the object on which the RFID device is mounted (active RFID). Recently, the researchers proposed solutions focused on the improvement of sensitivity and transmission range of tags (e.g., [1], [2]) as well as on the introduction of systems able to gather energy from the working environment of the devices to extend the lifetime of the batteries. At this regard, the research directions are oriented toward the development of energetically autonomous devices by means of an approach that combines Ultra Low Power (ULP) architectures (to limit the power consumption) with the capability to harvest energy from renewable sources available in the environment where the devices operate, like vibrations, thermal gradients or light. Compared to these energy sources, the use of power radiated by RF signals prevents dependency on the variable (and uncontrollable) environmental conditions [3], [4], because the RF energy for the remote power supply can be ad-hoc generated.

This has significantly increased the interest in remote powering systems for low-power applications such as wireless sensors. The main limitation of this technology is the very low power available at far locations, which can also vary significantly with the distance from the power source and the antenna orientation [5]. This requires to implement circuit and system solutions for the whole sensor systems and the RF-DC power converters capable to operate at ultra-low power level with the maximum sensitivity and efficiency [6]–[10]. RF-DC converter solutions proposed in the literature so far were mostly focused on the improvement of circuit performances without properly accounting for application related issues such as the input power variations and the misalignment between RF power transmitter and receiver, which severely penalize output power and efficiency [11], [12]. These are typical working conditions of systems using interchangeable implements and having more than one degree of freedom (e.g., robotic arms, manipulators, car transportations systems, earthmoving machineries or telehandlers), where both distance and orientation between RF power transmitter and receiver can vary unpredictably during the normal operation of the machinery on which they are mounted.

In this scenario, the system proposed in this paper contributes to overcome these issues and aims to be the starting point toward the implementation of more complex systems enabling the introduction of new safety functions as well as the improvement of the functions already present in machineries with interchangeable implements.

As described in the following, the proposed system had been applied to the real case study of the automatic identification of implements connected to a telehandler. The system is comprised of two devices: the IGD installed on the free end of the telescopic arm of the telehandler and the ED mounted on the implement. Differently from other similar systems used for automatic identification of implements, (e.g., [13]), the proposed system embeds a RF power delivery system compliant with the regulations currently in force in Europe and North America. The RF power delivery system integrated with the entire electronic system, had been designed through a comprehensive methodology that accounts for both the RF-DC converter and the antenna. Its design taken into account also boundary conditions of real industrial scenarios that further affect the efficiency of the power transfer (e.g., the devices will be reasonably fixed on metallic brackets made of aluminum or steel, the devices will be embedded in a plastic housing for protection reasons).

Moreover, the proposed system provides also the effective working time and the key parameters (e.g., dimensions, weight, barycenter, maximum load capacity, etc. . .) of the connected implement to the main ECU of the vehicle, that can use them for both programmed maintenance and safety related purposes (i.e., improvement or introduction of active safety functions).

Summarizing, the main contributions of the paper are the following. First, it presents a system for the automatic identification of implements connected to a main vehicle enabling the consequent improvement of the safety functions already available in the main ECU (e.g., control stability algorithms can now take into account information of the working condition of the whole machinery and can update dynamically their input parameters accordingly with the connected implement). Second, combining ULP consumption and RF energy harvesting capabilities, the paper shows as it is possible to obtain an easy-to-install system with extended battery lifetime compared with classic wireless devices, able to enhance active safety functions also in case of use of very old implements with no other electronic devices on board.

The paper is organized as follows. Section II presents the proposed system architecture. Section III and Section IV describe the power management policy and the main characteristics of the implemented communication protocol, respectively. Experimental results are presented in Section V, while Section VI concludes the paper.

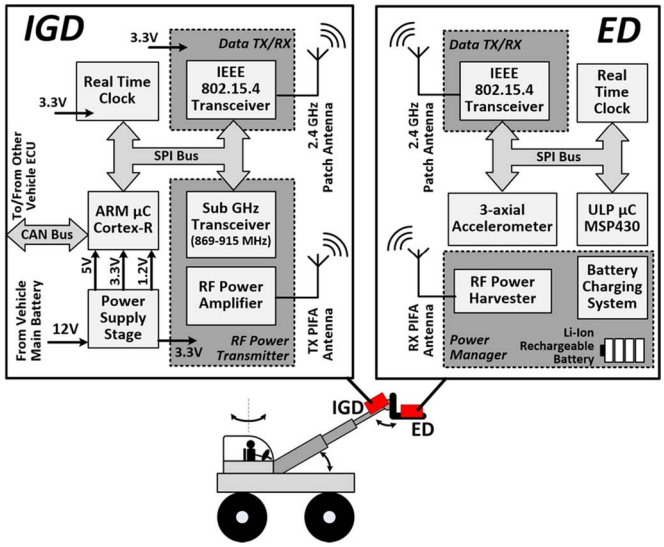

Fig. 1. Simplified block diagram of the proposed system with the main functional blocks of the IGD and ED highlighted. When the implement is physically connected to the telehandler, its ED starts a linking procedure with the IGD. If the implement is recognized as one of those fully compatible with the telehandler, the linking procedure successfully ends, and the normal operation of the system can start (see Section IV for a detailed description). Conversely, a warning message is notified to the operator.

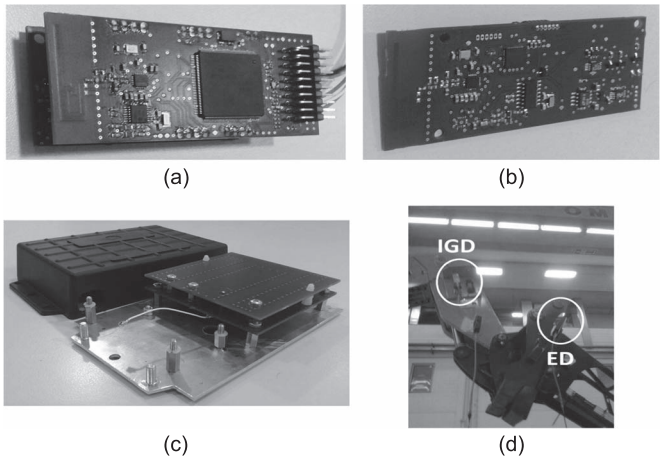

Fig. 2. Implemented prototypes. (a) IGD prototype. (b) ED prototype. (c) PIFA with aluminum cover and plastic housing. Two prototypes have been realized. The first prototype is used for the IGD, whereas the second prototype is used for the ED. The free space is reserved for the electronic circuitry (ED or IGD). (d) System mounted on a real telehandler. The IGD is mounted on the free end of the telescopic arm of the telehandler, whereas the ED is mounted on the connected implement.

II. System Architecture

As shown in Fig. 1, the proposed system had been applied to the real case study of the automatic identification of implements connected to a telehandler.

The system is comprised of two main devices: the Illuminator-Gateway Device (IGD), mounted on the free end of the telescopic arm of the telehandler, and the End Device (ED), mounted on the connected implement.

The IGD has two functions: i) it operates as gateway for data exchange between ED and any other Electronic Control Unit (ECU) of the vehicle using a standard CANopen communication; ii) it generates the RF power signal used for the remote powering of the ED. The transmitted RF power signal is compliant with both the regulations in force in EU and North America (ETSI 300-220, [14], and FCC part 15.247, [15], respectively).

The ED, instead, is in charge to send the unique identifier (ID) and the specific parameters of the implement on which it is mounted to the IGD by means of a 2.4 GHz bidirectional wireless link. The specific implement parameters (i.e. ID, size, weight, maximum load, etc...), are preloaded in the ED at programming time and, for safety reasons, cannot be modified by the operator of the telehandler.

When the implement is physically connected to the telehandler, the ED requests to be linked to the IGD. The linking procedure is completed only after that the implement ID (provided by ED) had been recognized by the IGD as one of those compatible with the telehandler on which the IGD is mounted. The check is performed by the main ECU of the vehicle, which controls that the operation limits of the implement on duty (e.g., maximum height and maximum extension of the telescopic arm, maximum load, etc...) are compliant with the maximum operating limits of the machinery. If the connected implement is not fully compatible with the telehandler, a warning message is notified to the operator to inform him about a potentially dangerous working condition derived from the use of a not compatible implement.

Once the implement-telehandler compatibility check is successfully completed, the ED can start the computation of the effective working time of the implement. The working time is periodically transmitted to the IGD together with its unique ID and used for programmed maintenance purposes.

In order to determine the effective working time of the implement, two concurrent events have to happen: i) the presence of persistent vibrations on the ED, detected by means of a 3D accelerometer integrated on the device; ii) a successful IGD-ED connection had been established.

The ED embeds also an RF energy harvesting circuit that collects and converts the RF energy delivered by the IGD. The energy gathered by the harvester is handled by a power management circuit that supplies the ED during its normal operation, and recharges a Li-Ion backup battery in case of surplus of incoming RF energy.

Both IGD and ED use a customized dual band Planar Inverted Folded Antenna (PIFA) to implement the required RF power link. The antenna had been designed and optimized to work at both 869 MHz and 915 MHz, compliant with EU and North America regulations respectively.

Fig. 2 shows the implemented prototypes of ED, IGD and PIFA that are described in detail in the following subsections.

A. Illuminator-Gateway Device (IGD) With Embedded RF Power Transmitter

The simplified architecture of the IGD is shown in Fig. 1. The core of the IGD hardware architecture is a Texas Instruments ARM Cortex-R microcontroller with a dual core lockstep CPU and clock frequency up to 220 MHz, single bit error correction

and double bit error detection. The IGD is designed to be compliant with the IEC 61508 regulation.

As mentioned above, the IGD is in charge of two main tasks. The first one is to operate as gateway in the data exchange between the ED and any other electronic devices on the vehicle (e.g., other ECUs). To do this, the IGD uses a 250 Kbps CANopen based protocol, while the wireless communication between IGD and ED is implemented using a 2.4 GHz low-power and IEEE 802.15.4 compliant transceiver (i.e., CC2500 from Texas instruments) with a customized patch antenna.

The implement parameters received from the ED are used to check if the implement is compatible with the telehandler on which the IGD is mounted. If there is a positive match, the IGD completes successfully the linking procedure with the ED and the normal operation of the system can start. Vice versa, the linking procedure is aborted and a warning message informs the operator about a potentially dangerous working condition derived from the use of an implement not fully compatible with the telehandler.

Furthermore, the IGD warns about the need of maintenance of the connected implement according to the effective working time of the implement received from the ED. The Real Time Clock (RTC) integrated in the IGD is used for the consistency check of both counter and calendar data sent by the ED.

The second task performed by the IGD is the generation of the RF signal used to deliver the RF power to the ED. As mentioned before the RF power transmitter is compliant with both the regulations in force in Europe and North America.

The same hardware architecture is exploited for both the regulations. The changes needed to meet the two different RF power regulations are obtained by changing slightly the value of passive RF components and the IGD firmware. In particular, a different carrier frequency has to be set (i.e., 869.525 MHz for Europe or 915 MHz for North America) and a Frequency-Hopping Spread Spectrum (FHSS) algorithm has to be enabled for the North America regulation. The implemented FHSS algorithm uses 50 channels in the 914–916 MHz range, with a channel spacing of 40 KHz and dwell time of 400 msec for each channel.

The RF power signal delivered to the ED is generated by a sub-GHz transceiver (i.e., CC1120 from Texas Instruments), which is controlled by the microcontroller through a classic SPI communication. For both regulations the CC1120 output narrowband single-tone signals have been generated by configuring the transceiver in continuous transmission mode. The output signals have been amplified up to $+26$ dBm exploiting a CC1190 range extender from Texas Instruments.

In order to avoid useless transmissions, the RF power transmission starts only when an ED is detected and the IGD-ED linking procedure is successfully completed, and ends when the implement is physically disconnected from the telehandler (i.e., the ED is out of range and the IGD does not receive any more data packet from the ED).

B. End Device (ED) With RF Power Harvester

From the design point of view, the minimization of the power consumption of the ED is one of the most challenging tasks. For this purpose, an HW-SW co-design approach had been exploited. Only ULP components are used and every system resource is enabled only for the time strictly required to complete its tasks, being completely turned off for the rest of the time.

As shown in Fig. 1, the ED embeds a Texas Instruments MSP430F2274 ULP microcontroller and exploits the same hardware architecture of the IGD (i.e., CC2500 2.4 GHz transceiver with dedicated patch antenna) for the wireless data exchange with the ED.

With reference to the considered case study, the ED is in charge of two main functions. The first one is to provide the unique identifier of the implement and its main parameters (e.g., barycenter, weight, load capacity, etc. . .) needed to verify the compatibility between the implement and the telehandler. The second one is the count of the effective working time of the implement on which it is mounted. To perform this task it uses a Microchip MCP795W21 ULP Real Time Clock (RTC), that communicates with the microcontroller by sharing a classic SPI bus with the wireless transceiver and a STMicroelectronics LIS3DH ULP 3-axial accelerometer. The microcontroller awakens the accelerometer periodically to check the presence of vibrations. If vibrations with accelerations higher than 50 mg are detected (at least in one of the accelerometer axis), a potential working condition occurs, and the ED starts the linking procedure described in Section IV. The chosen threshold value has been obtained from an experimental characterization carried out by means of a high performance 3-axial accelerometer from PCB Piezotronics. The data have been, acquired by a NI compact RIO board and processed in a NI LabView environment. The measurements had been carried out on different implements connected to the telehandler when on duty and they were repeated with the accelerometer located in different positions for each considered implement. The chosen threshold of 50 mg results from the combination of two distinct aspects of the system design. The first one is the estimation of a unique threshold suitable for all the implements in order to keep the firmware of the ED as simple as possible. The second one is the choice of a threshold that minimizes the number of false working condition detections, which lead to an increase of the power consumption of the ED, because a RF data packet is sent each time that the ED wakes up to check the presence of an IGD, as described in Section IV.

Concerning the performances of the data link, we carried out some tests showing that there are no significant packet losses (PER less than 1%) at the used transmission rate of 250 KBaud. This occurs thanks to the high sensitivity of the CC2500 RF transceiver (i.e. -87 dBm, when it is configured for current optimization, like in our case). Moreover, the realized 2.4 GHz printed PCB antenna is omnidirectional and it is in charge to transfer data and not RF power, therefore the relative positioning of ED (transmitter) and IGD (receiver) is much more less critical. In addition, in the considered scenario, the distance between ED and IGD is very limited and although the PCB antenna presents a gain of about -2 dBi, the very high sensitivity of the CC2500 widely compensate for both misalignments between ED and IGD and the presence of objects in the signal path.

Finally, the ED embeds also a smart power management circuit described in detail in Section III. It represents a distinctive feature of the proposed system and it had been designed to optimize the use of the RF energy delivered by the IGD and harvested by the ED.

C. Planar Inverted Folded Antenna—PIFA

The antenna plays a key role to optimize the efficiency of the implemented remote RF power delivery system. Its design requires taking into account several factors related to the real environment where the system will work. In particular, the relative positioning between RF power transmitter and harvester, and the materials/structures (e.g., metals, etc.) in the proximity of IGD and ED are key aspects that must be considered in order to maximize the antenna performances. Since such characteristics are strictly application-dependent, a customization of the antenna is needed.

In the considered application, the relative positioning between ED and IGD may vary unpredictably. Indeed, when a telehandler is on duty, the extension and the working height of its telescopic arm can change continuously depending on the working tasks. At the same time, the connected implement may rotate to maintain the best working position. The implement rotation causes a variation of both distance and relative orientation between the antennas of IGD (i.e. RF power transmitter) and ED (i.e., RF power harvester). Consequently, to limit the impact of these variations on the performance of the RF power delivery system, both relative positioning of IGD and ED and antenna topology have to be accurately chosen.

Classic omnidirectional antennas reduce the impact of the misalignment on the performance of the system. However, their very low gain results in an high reduction in the amount of RF energy that can be harvested. Therefore, in order to improve the performance of the whole system, the use of a customized antenna designed to work efficiently in condition of no/poor alignment between RF transmitter and RF harvester is needed.

The implemented RF power link exploits the same antenna for both IGD and ED. It is a customized dual band Planar Inverted Folded Antenna (PIFA), optimized to operate at the frequencies of 869 MHz and 915 MHz, according to the regulations in force in Europe and North America, respectively. The PIFA consists of a ground plane connected with a top plate element by means of a feed wire and one or more shorting elements. The PIFA solution has the advantages of reduced sizes, large bandwidth and high antenna gain [16]. As demonstrated in [17]–[19], additional resonance frequencies can be easily obtained adding parasitic elements (patches) to the main patch of the top plate. The tuning of the desired resonance frequencies can be obtained by changing: i) the distance between top plate and ground plane, ii) the dimensions and the relative positions of the parasitic elements on the top plate, iii) the position of feed wire and shorts on the top plate, iv) the dielectric constant of the substrate, [20]–[24].

The effects of variation in the antenna directivity and asymmetries in the radiation diagram due to the parasitic elements of the PIFAs are usually undesired. Interestingly, they have been exploited in the design of the antenna to improve the power link efficiency in case of no/poor alignment between transmitting and receiving antenna.

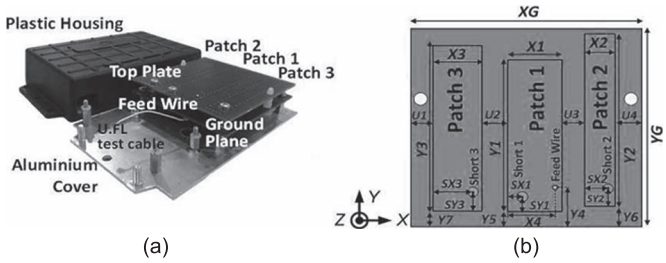

Fig. 3. Implemented Planar Inverted Folded Antenna (PIFA). (a) Picture of the prototype. (b) Sketch of the PIFA's top plate with the design parameters highlighted.

TABLE I
GEOMETRICAL DESIGN PARAMETERS OF THE PIFA'S TOP PLATE

	Value (mm)		Value (mm)		Value (mm)		Value (mm)		Value (mm)
X1	22.1	*Y2*	73.7	*Y7*	0.9	*SX1*	2.7	*SY3*	5.9
X2	10.7	*Y3*	68.3	*H*	8	*SX2*	6.9	*U1*	5.2
X3	15.3	*Y4*	9.8	H_{al}	12	*SX3*	10.6	*U2*	9.7
X4	19.3	*Y5*	0.9	*XG*	79	*SY1*	8.8	*U3*	9.3
Y1	64.3	*Y6*	2.3	*YG*	79	*SY2*	6.8	*U4*	6.7

Fig. 3 shows the implemented antenna and its geometric design parameters. The values, obtained from a parametric optimization procedure using a commercial electromagnetic simulator, are reported in Table I. The designed PIFAs have a square footprint of 79 $\times$ 79 mm and had been implemented using a commercial double side 1.6 mm thick FR4 substrate with copper thickness of 35 μm on each side. The distance between ground plane and top plate, H, is 8 mm, while the distance between the ground plane and aluminum cover of the plastic housing, H_{al}, is 12 mm. The choice of H and H_{al} is a trade-off between the bandwidth at the target frequencies and physical dimensions of the PIFA. The shorting elements have been realized using commercial braces of brass. The brass feed has a diameter of 1.02 mm.

III. POWER MANAGEMENT IN THE ED

A distinctive characteristic of the proposed system is that the ED is powered by the RF energy delivered by the power transmitter on the IGD. On the ED side, this requires an ad-hoc power conversion and management system, which had been embedded into the ED. The circuit schematic of the developed power conversion and management circuit is shown in Fig. 4. It is comprised of a RF energy harvester based on a commercial RF-DC converter (i.e., P2110 from Powercast) and a battery charger (i.e., LTC4070 form Linear Technology).

The RF-DC converter, in turn, is comprised of two main functional blocks: a voltage rectifier used to charge the external capacitor C_{STORE} by means of the RF energy harvested, and a output DC-DC converter exploiting the energy stored in C_{STORE} to provide a regulated DC voltage.

In order to ensure the service continuity also in case of no/few RF energy available a rechargeable Li-Ion battery has been added to the power supply stage of the ED.

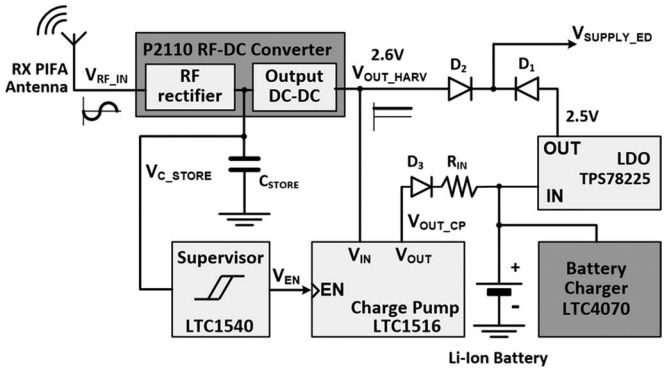

Fig. 4. Simplified block diagram of the ED power management circuit with the main functional blocks highlighted.

TABLE II
POWER MANAGEMENT POLICY

Condition	ED's Power Source	Battery Recharge
$E_{RF}(t) = 0$	Battery	No
$E_{RF}(t) \leq E_{Task}(t)$	Battery + RF harvester	No
$E_{RF}(t) > E_{Task}(t)$	RF harvester	Yes

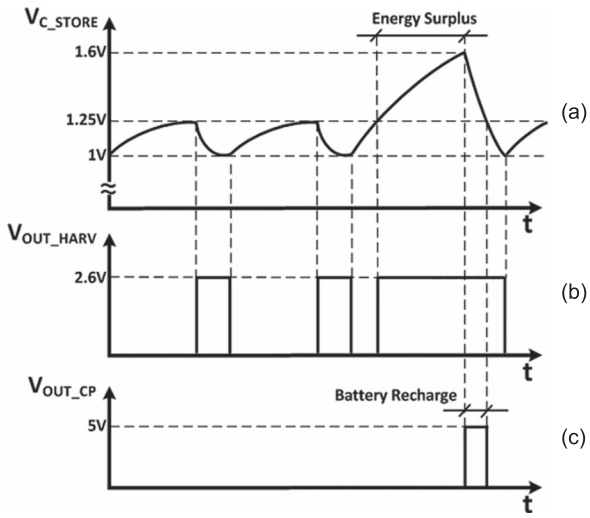

Fig. 5. Qualitative schematization of the basic operating principle of the implemented power management system through key waveforms (time axis not in scale). (a) Voltage across C_{STORE}. (b) RF-DC converter output voltage. (c) Charge pump output voltage.

The implemented power management policy aims to efficiently combine the RF energy harvested with the energy provided by the backup battery. It considers both the amount of collected RF energy available at a given instant of time, $E_{RF}(t)$, and the energy required by the ED to executes its current task at the same instant of time, $E_{\mathrm{Task}}(t)$. Table II summarizes the operating logic of the implemented power management circuitry. At a given instant of time, if no $E_{RF}(t)$ is available, the ED is fully powered by the backup battery. If $E_{RF}(t) \leq E_{\mathrm{Task}}(t)$ the ED is powered by both the RF energy harvester and the battery, which provides the remaining amount of energy $E_{\mathrm{Task}}(t) - E_{RF}(t)$ needed to execute the current task. Finally, if $E_{RF}(t) \geq E_{\mathrm{Task}}(t)$ the ED is fully powered by the RF energy harvester and the surplus of energy is used to recharge the backup battery. With the chosen power management policy the available $E_{RF}(t)$ is instantaneously used. This allows reducing both the circuitry complexity and the energy losses due to the leakage of additional hardware components needed to manage and store the harvested energy.

The operating principle of the power management circuitry designed to implement the above policy can be understood considering the qualitative waveforms shown in Fig. 5.

Under the assumption that the ED is in the working range of the IGD (i.e., a significant amount of RF energy is captured by the implemented RF antenna) and a RF power transmission is in progress, the voltage across C_{STORE}, i.e., V_{C_STORE}, rises (see Fig. 4). Until $V_{C\_\mathrm{STORE}} \leq 1.25$ V, the output of the RF-DC converter is disabled and the ED is powered by the back-up battery through the TPS78225 2.5 V Low Drop-Out (LDO) regulator from Texas Instruments. This condition occurs typically after a long time of inactivity of the implement on which the ED is mounted, or when, at a given instant, the energy requirement of the ED is higher than the amount of the energy harvested and stored in C_{STORE}.

Once V_{C_STORE} reaches 1.25 V, the output of the RF-DC converter, is enabled and its output voltage$V_{\mathrm{OUT_HARV}}$ is set to 2.6 V. Thanks to the diodes D_1 and D_2 (see Fig. 4), the ED is thus powered by the energy stored in C_{STORE}. If there is no RF power transmission in progress, or the energy requirement of the ED is higher than the amount of collected RF energy, V_{C_STORE} decreases.

When V_{C_STORE} reaches 1 V, the output of the RF-DC converter is disabled and the ED is powered again by the battery. Of course V_{C_STORE} decreases as quickly as higher is the difference between $E_{RF}(t)$ and $E_{\mathrm{Task}}(t)$.

If $E_{RF}(t) > E_{\mathrm{Task}}(t)$, V_{C_STORE} continues to rise above 1.25 V, and the energy in excess $E(t) = [E_{RF}(t) - E_{\mathrm{Task}}(t)]$ is used to recharge the battery through the implemented battery charging circuit. The average charging current, $I_{\mathrm{CHG\_AVG}}$, is defined by the input resistance of the battery charger, R_{IN}, according to (1)

$$I_{\mathrm{CHG\_AVG}} = \frac{V_{\mathrm{OUT\_CP}} - V_{\mathrm{BAT}}}{R_{\mathrm{IN}}} \tag{1}$$

where $V_{\mathrm{OUT\_CP}} = 5$ V is the output voltage of the charge pump circuit (i.e., LTC1516 from Linear Technology) used to boost the output voltage of the RF-DC converter, and $V_{\mathrm{BAT}} = 3.7$ V is the nominal voltage of the battery. For the considered case study $I_{\mathrm{CHG\_AVG}} = 2.7$ mA, with $R_{\mathrm{IN}} = 470\ \Omega$.

The charge pump is enabled by a supervisor circuit based on the LTC1540 ULP hysteresis comparator from Linear Technology. The supervisor continuously checks V_{C_STORE}, and enables the charge pumping circuit when $V_{C\_\mathrm{STORE}} = 1.6$ V. This value had been chosen according to the specifications of the commercial P2110 RF-DC converter used. Of course, V_{C_STORE} decreases during the battery recharge and when $V_{C\_\mathrm{STORE}} = 1.25$ V the exceeding energy has been completely used. The charge pump is disabled, while the output of the RF-DC converter, $V_{\mathrm{OUT\_HARV}}$, remains enabled until V_{C_STORE} reaches the lower bound (i.e., 1 V) continuing to provide energy to the ED.

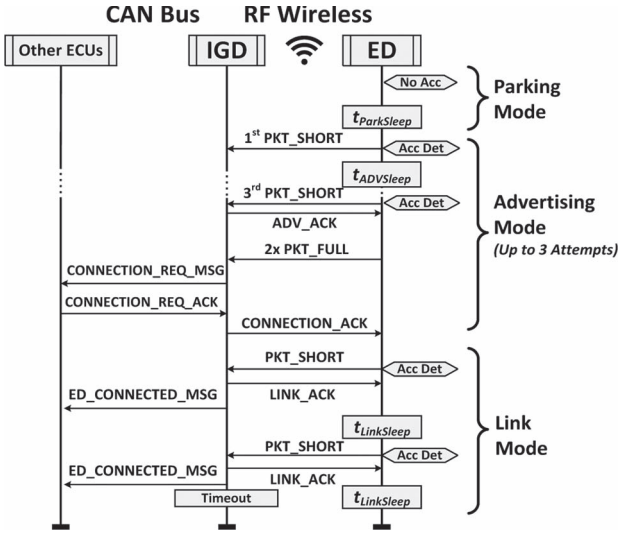

Fig. 6. Implemented Handshaking. Chronological sequence of messages exchanged among ED, IGD, and other vehicle's ECUs.

IV. Communication Protocol

The implemented communication protocol results from a tradeoff between two opposite requirements. From one hand, the safety critical application considered in this case study requires a robust bidirectional communication between IGD and ED. From the other hand, the highest power consumption occurs during data transmission and suggests minimizing both duration and the frequency of the data exchange between IGD and ED in order to obtain a self-powered ED.

The achieved tradeoff solution is based on the sequence diagram of Fig. 6, which shows all the tasks that have to be executed to establish a correct communication.

The communication protocol provides for three main functional modes: Parking Mode, Advertising Mode and Link Mode. Depending on the functional mode, specific data packets with different duty cycle and length have been designed in order to minimize the power consumption during the data exchange between IGD and ED. The format of the data packets can be customized at programming time according to the specific application needs.

During the inactivity period of the implement, the ED is in Parking Mode (PM). The microcontroller is in deep-sleep mode and all the peripherals are turned off with the exception of the RTC. The RTC awakes periodically the microcontroller every $t_{\mathrm{ParkSleep}}$ seconds. The generated interrupt is used to turn on the accelerometer that measures the 3-axial accelerations for approximately 1.3 seconds at a sampling rate of 100 Hz. If at least one of the measured accelerations is higher than 50 mg, a potential working condition is recognized and the ED enter in Advertising Mode (ADVM).

In Advertising Mode, the ED transmits a wireless data packet (PKT_SHORT) every t_{ADVSleep} seconds. The packet contains only the unique identifier of the ED and a minimal set of parameters identifying the implement. If no acknowledgment from the IGD is received after the transmission of the third PKT_SHORT the ED goes again in Parking Mode. Vice versa, if an IGD responds by sending an Acknowledgment Packet (ADV_ACK), the ED sends two consecutive full data packets (PKT_FULL) containing the full set of parameters of the implement (dimensions, barycenter, weight, load capacity, etc...) and the connection procedure can continue. The two PKT_FULL data packets contain the same information. The transmission is redundant in order to detect errors that may occur in the data transmission.

The IGD forwards the connection request coming from the ED and the parameters of the relative implement to the main ECU of the vehicle (CONNECTION_REQ_MSG). If the compatibility check is passed (CONNECTION_REQ_ACK) and no other connection procedure is ongoing, the IGD sends an acknowledgment packet (CONNECTION_ACK).

When in Link Mode (LM), the ED starts the count of the effective working time of the implement, checking periodically the presence of vibrations to verify that the implement is still on duty. The ED sends the updated count every $t_{\mathrm{LinkSleep}}$ seconds within the PKT_SHORT.

For each received PKT_SHORT, the IGD responds to the ED with a specific Acknowledgement Packet (LINK_ACK) that is used by the ED to check the operation status of the IGD. At the same time, the IGD forwards the updated data included into the received PKT_SHORT to the other ECUs of the vehicle (ED_CONNECTED_MSG) for continuous consistency checks between the implement on duty and the current operation of the telehandler. The use of PKT_SHORTs is twofold. First, it allows reducing the power consumption of the ED. In fact, in Link Mode, the implement is fully identified; therefore, there is no need to send the full set of data parameters. Second, it is used as "*alive message*" to check if the ED is working properly. Whenever a PKT_SHORT is received, the IGD sends back an Acknowledgement Message (LINK_ACK) to the ED.

The disconnection procedure, which brings the ED again into Parking Mode, starts if one of the following conditions occurs: i) no vibrations are detected by the ED at three consecutive interrogations; ii) no LINK_ACK messages are received by the ED within a defined timeout; iii) no PKT_SHORT messages are received by the IGD within a defined timeout.

In order to obtain a consistency check of the exchanged data a checksum field had been included in the data packet. Due to the extremely limited energy budget of the ED, the checksum algorithm had been chosen as simple as possible in order to limit the data transmission overhead and the additional power consumption. In particular, the data packet includes two special characters "$" and "$*$" at the beginning and at the end of the sensible data field, respectively. The checksum is calculated by an XOR of all characters in the message between, but not including, the two special characters. It is calculated by the data transmitter and by the data receiver using a mechanism very similar to the one used for the CRC consistency check in the CAN protocol. The data receiver checks if the received checksum code matches with its own checksum code calculated on the basis of the received data word delimited by the special characters "$" and "$*$." If there is agreement between the two checksum codes, the received data are unpacked. Vice versa, if there is no agreement the received message is discarded.

The robustness of the system has been further improved exploiting three of the main features of the transceiver used

(i.e., CC2500). The first feature is the classic Received Signal Strength Indicator (RSSI) mechanism. The second one is the Clear Channel Assessment (CCA) indicating if the current communication channel is free or busy. The CC2500 has been configured in TX-if-CCA mode to prevent multiple transmitter collisions in hardware starting a transmission only if the current channel is free. The third one is the Link Quality Indicator (LQI), that is a metric used as a relative measurement of the link quality and quality of the received signal used in combination with RSSI. Once enabled, the information provided by these three mechanisms are automatically used by the firmware functions included in the CC2500 driver at MRFI (Minimal RF Interface) level.

In addition, the system had been designed to allow only one linking procedure at a time between IGD and ED. Once an implement is linked with the IGD and is fully identified (i.e., the system is in Link Mode), the IGD discards any other connection request coming from other EDs. In this way, the system operates properly also when the whole machinery works very close to another machinery mounting another implement (or an implement of the same type, because the ID of the implements are unique), avoiding any kind of interference. From an application point of view, indeed, it is possible to have a working condition with two or more machineries working together to execute a defined task.

Interestingly, the wake-up mechanism of the ED and the start of the linking procedure between IGD and ED are based on the persistent presence of vibrations. This prevents from undesired linking requests due to accidental shocks on the implement and allows reducing the power consumption of the ED. Exploiting the ultra low-power consumption of the accelerometer, the additional power consumption due to a prolonged sensing time ($\sim$1 sec) is widely compensated by the large energy saving due to the smaller number of PKT_SHORT transmissions related to the reduction of the number of false working condition detections. As shown in the experimental results (see Section V), indeed, the power consumption of the accelerometer is in the order of 15 μA, three order of magnitudes lower than the power consumption of the RF transceiver in transmission mode.

The implemented start mechanism of the linking procedure allows to manage also other particular situations, e.g., IGD receives multiple connection requests when two (or more) implements are placed close to each other and are being fixed to two (or more) different telehandlers at the same time. In this case the IGD postpones the choice about the request to accept by a fixed time interval, until the request coming from the ED physically connected to the telehandler remains the only one and the linking procedure can be successfully completed. This occurs when the other EDs exit from their communication range, i.e., about 6 meters from the IGD with a transmission power of the CC2500 $P_{TX\_CC2500} = -4$ dBm (set at programming time of the ED).

V. Experimental Results

The system had been characterized by evaluating its functionality and by accurately measuring the performances of its key components. The measurements concerned: i) the complete characterization of the PIFA antennas used in the implemented RF power delivering system; ii) the power consumption of the ED in every working condition; iii) the performances of the RF energy harvester, to evaluate the capability of the ED to be powered only by the RF energy when in normal working conditions (i.e., Link Mode).

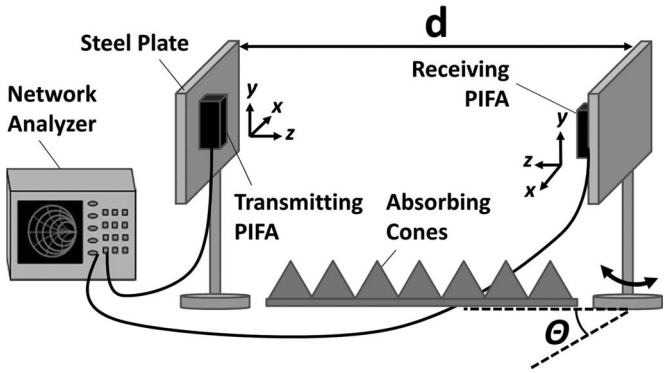

Fig. 7. Setup for PIFA S-parameters experimental measurements. Inaccuracy levels due to multipath fading affecting the wave propagation had been reduced by positioning the PIFAs at 2 m from the floor and 4 m from all the walls, with absorbing cones on the floor between the two antennas.

A. Antenna Characterization

Two prototypes of the designed PIFA antennas had been fabricated and characterized. In order to simulate real industrial scenarios, the prototypes have been encapsulated in a plastic housing with aluminum cover and fixed to a support with a commercial steel plate. The material properties of housing and fixture have been taken into account at the design phase of the PIFAs.

The prototypes had been characterized in laboratory, using the two-port setup shown in Fig. 7. An E5071C Network Analyzer is used to measure the return losses of the two antennas through the reflection coefficients S_{11} and S_{22}. The gain of the two antennas had been derived from the measured S_{21}, exploiting the Friis's formula shown in (2)

$$G = \sqrt{\frac{|S_{21}|^2}{\left(1-|S_{11}|^2\right)\left(1-|S_{22}|^2\right)\left(\frac{\lambda}{4\pi d}\right)^2}}, \quad \text{with } G = G_{TX} = G_{RX} \qquad (2)$$

This formula is valid under two reasonable assumptions: i) far field conditions (i.e., $D > 2\lambda$, where $D = 2$ m is the distance between the two antennas and 32.8 cm $\leq \lambda \leq$ 34.5 cm is the wavelength for the frequency range of interest); ii) both transmitting and receiving PIFA have the same gain G (i.e., $G = G_{TX} = G_{RX}$).

Fig. 8 shows measurements and simulations of the reflection coefficient S_{11} over the whole frequency range of interest. A very good agreement is observed between simulated and measured S_{11}, with a bandwidth of 10 MHz centered at 869 MHz and of 25 MHz around 915 MHz, both calculated considering a VSWR of 2:1 (i.e., $S_{11} < -9.5$ dB).

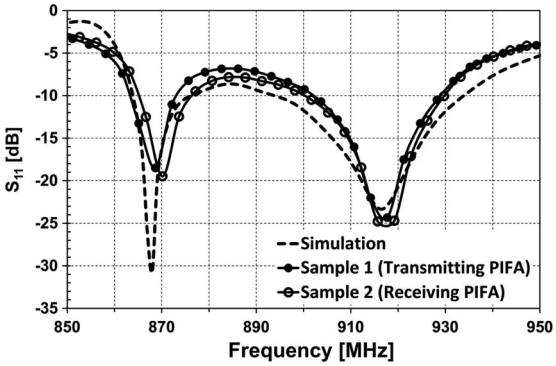

Fig. 8. Reflection coefficient S_{11}. Simulation results (dashed line) versus real measurements on the two implemented prototypes (solid lines with markers).

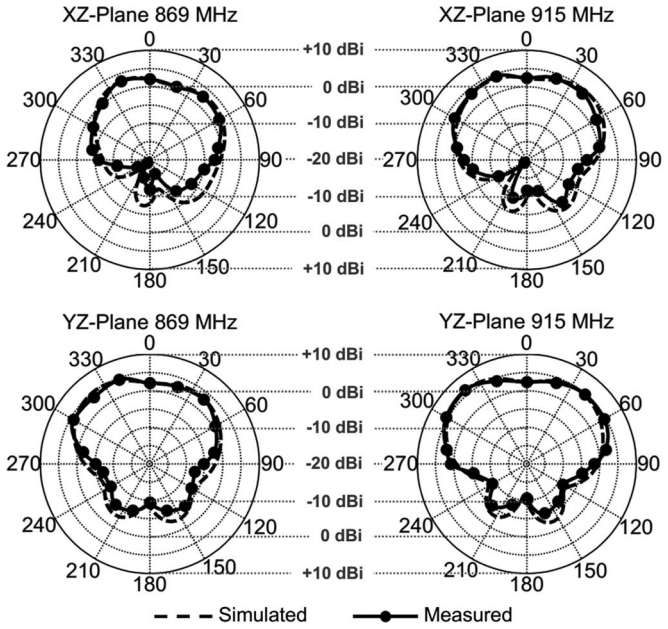

Fig. 9. Radiation diagrams: simulation results versus real measurements of the antenna gain at the frequencies of interest in the xz-plane and in the yz-plane.

Fig. 9 shows the simulated antenna gain of the receiving PIFA compared with the measured one for both the two frequencies of interest. The antenna gain, calculated from the measured S_{21} using (2), had been measured by rotating the receiving antenna around its vertical axis by different angles, Θ. The antenna prototypes show the highest gain in the xz-plane for variation of Θ, over a wide range of 120 degrees (-60 deg $\leq \Theta \leq +60$ deg), thus not requiring a perfect alignment between the two PIFAs to achieve optimum performances, in agreement with design expectations and system specifications.

With reference to Fig. 7, the setup used had only one degree of freedom, therefore the yz-plane plots have been obtained rotating both the PIFAs of 90 degrees and fixing them on the respective steel plate. As shown by Fig. 9, the highest performances have been obtained for a wide span of 120 degrees also in this configuration. In particular, the measured antenna gain is resulted higher than 0 dBi at 869 MHz and $+1$ dBi at 915 MHz

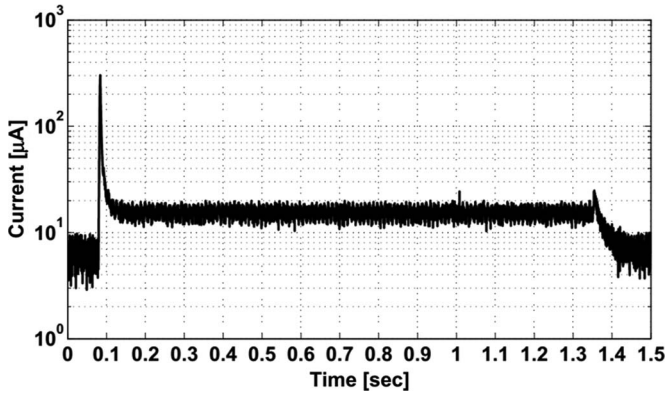

Fig. 10. Current consumption profile of the ED when in Parking Mode. When in deep sleep, the current consumption of the ED is only 5 μA mainly due to the current consumption of the RTC. During the awakening of the accelerometer, the current consumption peaks up to 300 μA, whereas at 1.3 s of the accelerations measurement, it is 15 μA on average.

for a wide range of radiation angle, peaking at $\sim$2 dBi and $\sim$4 dBi, respectively.

Interestingly, including a second parasitic element in the top plate of the PIFA allows obtaining a more symmetrical behavior of both gain and directivity of the PIFA compared with the classic 1-parasitic element implementation of dual band PIFAs.

B. ED Characterization

The ED current consumption had been measured for each operating mode of the device (i.e., Parking Mode, Advertising Mode and Link Mode). The measurements were carried out by means of a N6784A battery drain module integrated into a N6705B DC power analyzer from Agilent Technologies with dedicated 14585A Analysis Software.

Fig. 10 shows the current consumption profile of the ED in Parking Mode. The ED remains in deep sleep for the most of the time with a measured average current consumption $I_{\mathrm{DeepSleep\_avg}} = 5$ μA, while it wakes up every $t_{\mathrm{ParkSleep}} =$ 30 sec to check the presence of vibrations. The measurement lasts approximately, $t_{\mathrm{ACC}} = 1.3$ sec with an average current consumption, $I_{\mathrm{ACC\_avg}}$ of 15 μA, peaking up to 300 μA during the 10 msec of the accelerometer awaking. Of course, the total average current consumption of the ED in Parking Mode, $I_{\mathrm{Park\_avg}}$, depends on $t_{\mathrm{ParkSleep}}$. With the considered one, $I_{\mathrm{Park\_avg}}$ is $\sim$5.5 μA.

Once vibrations higher than 50 mg are detected, a potential working condition occurs and the ED enters in Advertising Mode. In this phase the ED checks the presence of an IGD every $t_{\mathrm{AdvSleep}} = 5$ sec. It wakes up from the deep sleep mode and sends a data packet (i.e., PKT_SHORT) containing only the ID and the basic parameters of the associated implement.

The relative ED current consumption profile is shown in Fig. 11(a). The data transmission of a PKT'SHORT and its related computations lasts approximately $t_{\mathrm{TxPktShort}} = 40$ msec with an average current consumption, $I_{\mathrm{TxPktShort\_avg}}$, of 17 mA peaking up to 23 mA. With the considered t_{AdvSleep} the average current consumption of the ED is $\sim$ 140 μA. If an IGD notifies its availability, the ED sends the full data packet

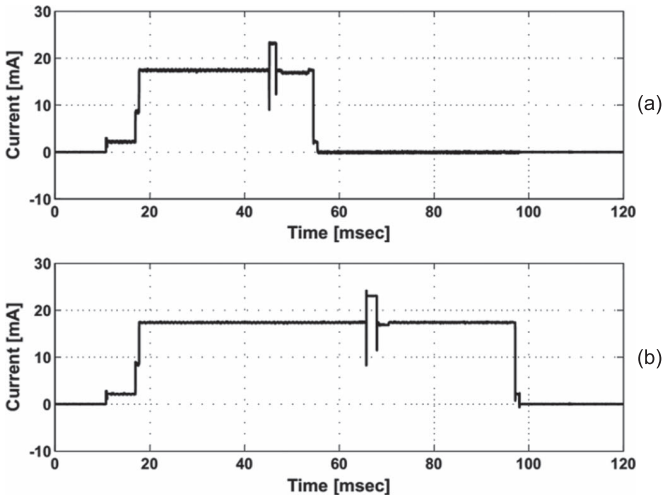

Fig. 11. Current consumption of the ED when in Advertising and Link Modes. (a) Current profile of the transmission of PKT_SHORT during the first stage of the Advertising Mode and the normal operation of the Link Mode. (b) Current profile of the transmission of PKT_FULL during the final stage of the connection procedure in Advertising Mode.

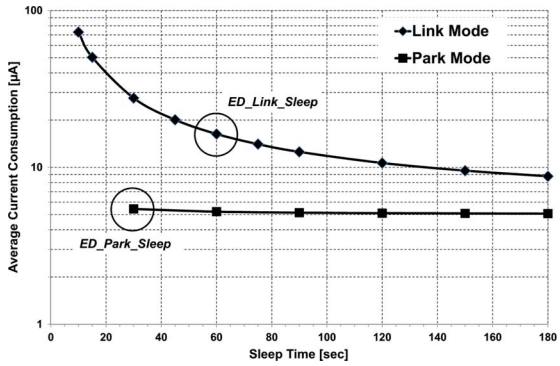

Fig. 12. Estimation of the average current consumption of the ED in Link Mode and Park Mode (i.e., $I_{\mathrm{Park\_avg}}$ and $I_{\mathrm{Link\_avg}}$) for different deep-sleep time intervals (i.e., $t_{\mathrm{ParkSleep}}$ and $t_{\mathrm{LinkSleep}}$). The values used in this paper are highlighted in figure.

containing the whole set of implement parameters on which the ED is mounted (PKT_FULL). As shown in Fig. 11(b), the total task lasts approximately $t_{\mathrm{TxPktFull}} = 90$ msec while the average current consumption is approximately 17 mA.

Once the IGD-ED linking procedure had been successfully completed, the ED enters in Link Mode, which is the normal operation mode of the system.

The ED sends a PKT_SHORT every $t_{\mathrm{LinkSleep}} = 60$ sec and the message includes the effective working time of the implement updated at each transmission. Of course, the average current consumption in Link Mode, $I_{\mathrm{Link\_avg}}$, drops significantly to 17 μA, due to the longest sleeping time between two consecutive PKT'SHORT transmissions.

The time intervals $t_{\mathrm{ParkSleep}}$, t_{ADVSleep}, and $t_{\mathrm{LinkSleep}}$, can be set at programming time and have to be chosen as a tradeoff between the timing requirements of the specific application and the power consumption of the ED, which, of course, decreases with lowering the application duty cycle. It is reasonable to assume that the ED spent the most of the time in either Parking Mode or in Link Mode, hence the choice of $t_{\mathrm{ParkSleep}}$ and $t_{\mathrm{LinkSleep}}$ has the larger impact on the power consumption of the ED.

Starting from the measured $I_{\mathrm{Park\_avg}}$ and $I_{\mathrm{Link\_avg}}$, the influence of the relative sleep time intervals on the system performance had been estimated through (3) and (4), shown at the bottom of the page. Results of Fig. 12 show that the frequency of the vibration check does not have any substantial impact on $I_{\mathrm{Park\_avg}}$ due to the extremely low consumption of the accelerometer, which is of the same order of magnitude of the RTC (i.e., the only peripheral of the ED "*always ON*"). Therefore a $t_{\mathrm{ParkSleep}} = 30$ sec had been chosen to keep a good reactivity of the system. Vice versa, due to the very high current consumption during the data packet transmission, the $t_{\mathrm{LinkSleep}}$ had been chosen as best trade-off between current consumption and precision in the effective working time notification.

C. RF Energy Harvester Characterization

The performances of the RF energy harvester embedded in the ED have been characterized by comparing the harvested RF power to the average ED power consumption in Link Mode. This allows to evaluate the degree of energy autonomy (or self-sustainability) of the ED in Link Mode operation, i.e., the only functional mode where RF energy is delivered by the IGD to the ED.

The figure of merit adopted to evaluate the performance of the RF energy harvester is given by the ratio between the average current provided by the RF energy harvester and the average current absorbed by the ED during its operation, $I_{\mathrm{Link\_avg}}$.

In real applications, the amount of power effectively delivered to the ED depends on two factors that must be accurately taken into account: i) the IGD cannot provide RF power continuously due to the regulations currently in force; ii) the amount of RF power harvested by the ED is not constant because it depends on the distance and on the relative alignment between IGD and ED, which may vary significantly during the normal operation of the implement.

For these reasons, in order to characterize the RF energy harvester performances, the setup sketched in Fig. 13 had been realized. It emulates the relative misalignment between ED and IGD antennas occurring during the normal operation of the

$$I_{\mathrm{Park\_avg}} = \frac{I_{\mathrm{ACC\_avg}} \cdot t_{\mathrm{ACC}} + I_{\mathrm{DeepSleep\_avg}} \cdot (t_{\mathrm{ParkSleep}} - t_{\mathrm{ACC}})}{t_{\mathrm{ParkSleep}}} \tag{3}$$

$$I_{\mathrm{Link\_avg}} = \frac{I_{\mathrm{TxPktShort\_avg}} \cdot t_{\mathrm{TxPktShort}} + I_{\mathrm{DeepSleep\_avg}} \cdot (t_{\mathrm{LinkSleep}} - t_{\mathrm{TxPktShort}})}{t_{\mathrm{LinkSleep}}} \tag{4}$$

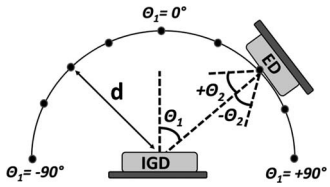

Fig. 13. Setup used for the RF energy harvester characterization.

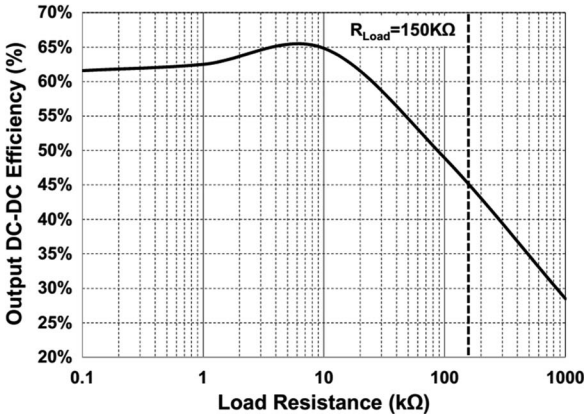

Fig. 14. Efficiency of the RF harvester output DC–DC converter. It is 45% for the equivalent input resistance of the ED ($R_{\rm Load} = 150$ kΩ).

implement connected to the telescopic arm of the telehandler. The IGD had been kept in a fixed position while the ED had been positioned at different distances d and angles θ_1 from the IGD. For each relative position, identified by (d, θ_1), three different measurements have been performed rotating the ED around its vertical axes at different angles θ_2.

The ED power consumption at a given time depends strongly on the task under execution. It afflicts the equivalent impedance at the output of the RF harvester which in turn varies from few kΩ (e.g., when the ED communicates with the IGD) to hundreds of kΩ (e.g., when the ED is in deep sleep).

In Link Mode, the measured average current consumption of the ED is $I_{\rm Link\_avg} = 17$ μA, while the regulated output voltage of the DC-DC converter embedded in the commercial P2110 RF harvester is 2.6 V. In first approximation, the equivalent resistance of the ED in Link Mode is thus given by $R_{\rm Load} = 2.6$ V/ 17 μA ≈ 150 kΩ.

Fig. 14 shows the efficiency of the output DC-DC converter plotted vs. different values of $R_{\rm Load}$ for a 2.6 V output voltage. As shown, to the average ED power consumption in Link Mode (i.e., $R_{\rm Load} = 150$ kΩ) corresponds an efficiency of the DC-DC converter $\eta_{DC-DC} = 45\%$;, which strongly affects the overall system efficiency.

Measuring the time $t_{\rm chrg}$ needed to charge the 1 mF storage capacitor $C_{\rm STORE}$, and using the estimated $\eta_{DC-DC} = 45\%$ it has been possible to calculate the average current available at the output of the RF energy harvester, $I_{\rm Harv\_avg}$, using (5)

$$I_{\rm Harv\_avg} = \frac{1}{2} C_{\rm STORE} \left(V_{CS\_H}^2 - V_{CS\_L}^2\right) \frac{1}{t_{\rm chrg}} \frac{1}{V_{\rm out\_harv}} \eta_{DC-DC} \quad (5)$$

TABLE III
PERCENTAGE OF SELF-SUSTAINABILITY SED OF THE ED WHEN IN LINK MODE FOR DIFFERENT RELATIVE POSITIONS BETWEEN IGD AND ED IN CASE OF SYSTEM COMPLIANT WITH REGULATION IN FORCE IN EUROPE

		Distance between IGD and ED					
		d = 35cm			*d = 50cm*		
	Θ_2 *[deg]*	*-45*	*0*	*+45*	*-45*	*0*	*+45*
Θ_1 [deg]	*-90*	N/A[a]	17.30	25.99	N/A[a]	N/A[a]	13.29
	-67.5	7.99	24.87	50.71	7.91	4.07	25.86
	-45	14.63	37.85	62.93	3.01	12.32	23.74
	-22.5	5.65	31.09	60.04	13.22	12.93	32.85
	0	13.71	23.53	45.82	3.17	4.08	17.83
	+22.5	20.81	16.37	23.32	13.60	N/A[a]	8.11
	+45	15.97	9.12	5.42	N/A[a]	N/A[a]	N/A[a]
	+67.5	10.08	N/A[a]	N/A[a]	N/A[a]	N/A[a]	N/A[a]
	+90	N/A[a]	N/A[a]	N/A[a]	N/A[a]	N/A[a]	N/A[a]

[a] N/A = $S_{ED} < 3\%$

where $V_{CS\_L} = 1$ V and $V_{CS\_H} = 1.25$ V are the threshold voltages required by the P2110 RF harvester, enabling and stopping the $C_{\rm STORE}$ charge, respectively; while $V_{\rm out\_harv} =$ 2.6 V is the DC regulated output voltage of the RF harvester.

Exploiting the measured average current consumption of the ED in Link Mode, $I_{\rm Link\_avg}$, and the calculated $I_{\rm Harv\_avg}$ it is easy to calculate the percentage of self-sustainability of the ED, S_{ED}, using (6)

$$S_{ED}[\%] = 100 \frac{I_{\rm Harv\_avg}}{I_{\rm Link\_avg}}. \quad (6)$$

The S_{ED}, evaluated in the case of RF power delivery compliant with the EU regulation and for different distances and orientation angles between IGD and ED, are reported in Table III. The implemented RF energy harvesting system supplies a significant amount of energy to the ED in a wide range of configurations (d, θ_1, θ_2). In particular, in case of optimal relative positioning between IGD and ED, the 63% of the average power required by the ED in Link Mode is provided by the realized RF harvester. In other words, this means that the proposed system contributes to extend the battery lifetime of the ED accordingly with (7)

$$T_{H+B} = T_B(1 + S_{ED}) \quad (7)$$

where T_B is the battery lifetime in case of ED completely powered by the battery and T_{H+B} is the lifetime of the battery in case of RF energy harvester that contributes to the power supply of the ED.

Similar results have been obtained also in the case of IGD configured to deliver RF power at the frequency of 915 MHz, compliant with regulation in force in North America.

The obtained results can be used also to identify the optimal relative positioning between RF power transmitter (i.e., IGD) and RF power harvester (i.e., ED). This is an issue strictly dependent on the specific implement and it has to be taken into account in the choice of the placement of the ED on the implement.

VI. Conclusion

The case study of automatic identification of implements connected to a telehandler had been used to demonstrate how the proposed system can enable the active and pre-crash safety enhancement in industrial vehicles as well as in every machinery that uses interchangeable implements.

The developed platform gives the possibility to exchange data between main vehicle and implement. Consequently, it allows recognizing the presence or not of a connected implementing and identifying its characteristic parameters. This, in turn, enables the implementation of additional safety functions (e.g., the use of optimal load charts for every implement in use and for every working condition, improving both safety and productivity), as well as the optimization of the existing ones (e.g., optimization of the control stability algorithms running on the main ECU by means of the real-time update of their input parameters according with the specific characteristics of the connected implement).

The whole system, comprised of two different wireless devices (i.e., the IGD, mounted on the free end of the telehandler's arm, and the ED mounted on the implement) had been developed following a hardware-software co-design methodology. Differently from other solutions proposed in the literature, a complete RF power delivering system, compliant with the regulations in force in Europe and North America, had been embedded in the system in order to increase the battery lifetime of the ED. The RF power transmitter had been integrated in the IGD, while the RF energy harvesting system had been integrated in the ED. The performances of the RF power link had been improved thanks to the use of two *ad-hoc* dual band PIFA antennas optimized to work efficiently for a wide range of orientation angles between IGD and ED.

Finally, the experimental results shown as the lifetime of the ED's battery had been increased up to the 63% (in case of optimal relative positioning between the IGD and the ED), thanks to the combination of the RF energy harvesting capabilities of the ED with its Ultra Low-Power architecture and the implemented power management policy.

References

[1] Y. Chia-Yu and H. Wei-Chun, "A 21.2-dBm dual-channel UHF passive CMOS RFID tag design," *IEEE Trans. Circuit Syst. I, Reg. Papers*, vol. 61, no. 4, pp. 1269–1279, Apr. 2014.

[2] L. Hyung-Min and M. Ghovanloo, "A high frequency active voltage doubler in standard CMOS using offset-controlled comparators for inductive power transmission," *IEEE Trans. Biomed. Circuits Syst.*, vol. 7, no. 3, pp. 213–224, Jun. 2013.

[3] C. R. Valenta and G. D. Durgin, "Harvesting wireless power: Survey of energy-harvester conversion efficiency in far-field, wireless power transfer systems," *IEEE Microw. Mag.*, vol. 15, no. 4, pp. 108–120, Jun. 2014.

[4] L. Xiao, P. Wang, D. Niyato, D. Kim, and Z. Han, "Wireless networks with RF energy harvesting: A contemporary survey," *IEEE Commun. Surveys Tuts.*, vol. 17, no. 2, pp. 757–789, 2nd Quart. 2015.

[5] Z. Popovic *et al.*, "Scalable RF energy harvesting," *IEEE Trans. Microw. Theory Techn.*, vol. 62, no. 4, pp. 1046–1056, Apr. 2014.

[6] S. Scorcioni, A. Bertacchini, and L. Larcher, "A 868 MHz CMOS RF-DC power converter with 17 dBm input power sensitivity and efficiency higher than 40% over 14 dB input power range" in *Proc. ESSCIRC*, 2012, pp. 109–112.

[7] J.-P. Curty, N. Joehl, F. Krummenacher, C. Dehollain, and M. J. Declercq, "A model for μ-power rectifier analysis and design," *IEEE Trans. Circuit Syst. I, Reg. Papers*, vol. 52, no. 12, pp. 2771–2779, Dec. 2005.

[8] R. E. Barnett, L. Jin, and S. Lazar, "A RF to DC voltage conversion model for multi-stage rectifiers in UHF RFID transponders," *IEEE J. Solid-State Circuits*, vol. 44, no. 2, pp. 354–370, Feb. 2009.

[9] Z. Hameed and K. Moez, "A 3.2 V -15 dBm adaptive threshold-voltage compensated RF energy harvester in 130 nm CMOS," *IEEE Trans. Circuit Syst. I, Reg. Papers*, vol. 62, no. 4, pp. 948–956, Apr. 2015.

[10] M. Pasca *et al.*, "A -19 dBm sensitivity integrated RF-DC converter with regulated output voltage for powering UHF wireless sensors," in *Proc IWASI*, 2015, pp. 168–171.

[11] C. Merz, G. Kupris, and M. Niedernhuber, "Design and optimization of a radio frequency energy harvesting system for energizing low power devices," in *Proc. AE*, 2014, pp. 209–212.

[12] Z. Popovic, E. A. Falkenstein, D. Costinett, and R. Zane, "Low-power far-field wireless powering for wireless sensors," *Proc. IEEE*, vol. 101, no. 6, pp. 1397–1409, Jun. 2013.

[13] A. Calcante and F. Mazzetto, "Design, development and evaluation of a wireless system for the automatic identification of implements," *Comput. Electron. Agriculture*, vol. 101, pp. 118–127, Feb. 2014.

[14] *Electromagnetic Compatibility and Radio Spectrum Matters (ERM);Short Range Devices (SRD); Radio Equipment to be Used in the 25 MHz to 1000 MHz Frequency Range With Power Levels Ranging up to 500 mW*, ETSI EN 300 220-1 V2.4.1, 2012.

[15] §15.247—Operation Within the Bands 902–928 MHz, 2400–2483.5 MHz, and 5725–5850 MHz, FCC, 2015.

[16] K. L. Virga and Y. Rahmat-Samii, "Low-profile enhanced-bandwidth PIFA antennas for wireless communications packaging," *IEEE Trans. Microw. Theory Techn.*, vol. 45, no. 10, pp. 1879–1888, Oct. 1997.

[17] H. T. Chattha, Y. Huang, Y. Lu, and X. Zhu, "Further bandwidth enhancement of PIFA by adding a parasitic element," in *Proc. LAPC*, 2009, pp. 213–216.

[18] K. Dong-Yeon, J. W. Lee, C. Choon-Sik, and K. Jaeheung, "A compact tri-band PIFA with multiple-folded parasitic elements," in *Proc. Int. IEEE/MTT-S*, 2007, pp. 259–262.

[19] C. R. Rowell and R. D. Murch, "A compact PIFA suitable for dual-frequency 900/1800-MHz operation," *IEEE Trans. Antennas Propag.*, vol. 46, no. 4, pp. 596–598, Apr. 1998.

[20] H. T. Chattha, Y. Huang, Y. Lu, and Z. M. Huang, "A study of parameter changes on the characteristics of planar inverted-F antenna," in *Proc. EuCAP*, 2009, pp. 370–373.

[21] H. T. Chattha, Y. Huang, and Y. Lu, "A further study of planar inverted-F antenna," in *Proc. IWAT*, 2009, pp. 1–4.

[22] C. Hua-Ming Chen and L. Yi-Fang, "Experimental and simulated studies of planar inverted-F antenna," in *Proc. IWAT*, 2005, pp. 299–302.

[23] H. F. Abu Tarboush, D. Budimir, R. Nilavalan, and H. S. Al-Raweshidy, "Wide-band planar inverted-F antenna for cognitive radio," in *Proc. EuMC*, 2009, pp. 1504–1507.

[24] Z. Yingbin, Y. Min, L. ShuFang, and X. Shuguang, "Investigations of specific absorption rate for dual-band PIFA antennas," in *Proc. ISAPE*, 2008, pp. 323–326.

Alessandro Bertacchini (M'06) was born in 1974. He received the Master's degree in computer science and the Ph.D. degree in industrial management engineering from the University of Modena and Reggio Emilia, Modena and Reggio Emilia, Italy, in 2001 and 2005, respectively.

He is currently an Assistant Professor with the University of Modena and Reggio Emilia. He has authored and coauthored several peer-reviewed technical papers on his topics of interest. His research interests include the design of embedded systems for industrial and safety-critical applications and the development of low-power energy harvesting systems.

Giacomantonio Napoletano was born in Italy in 1986. He received the Master's degree in electronic engineering from the Università della Calabria, Arcavacata di Rende, Italy, in 2010.

He has authored and coauthored several peer-reviewed technical papers on his topics of interest. His research interests include the development of embedded systems and smart sensors for industrial applications.

Stefano Scorcioni was born in Italy in 1984. He received the Master's degree in electronics engineering and the Ph.D. degree in information and communication technologies from the University of Modena and Reggio Emilia, Modena and Reggio Emilia, Italy, in 2005 and 2009, respectively.

He has authored and coauthored several peer-reviewed technical papers on his topics of interest. His research interests include ultralow-power wireless embedded systems design and the development of radio-frequency energy harvesting systems.

Luca Larcher (S'99–M'01) was born in Italy in 1972. He received the Ph.D. degree in information engineering from the University of Modena and Reggio Emilia, Modena and Reggio Emilia, Italy, in 2001.

He is currently an Associate Professor with the University of Modena and Reggio Emilia. He has authored a book and more than 140 technical papers. His research interests include the characterization and physical modeling of nonvolatile memory devices and charge transport in high-k dielectrics and the design of complementary metal–oxide–semiconductor integrated circuits for communication and energy harvesting.

Dr. Larcher has joined the Technical Committee of the International Electron Devices Meeting, International Reliability Physics Symposium, and International Integrated Reliability Workshop conferences.

Paolo Pavan (M'95–SM'12) received the Ph.D. degree in electrical engineering from the University of Padova, Padova, Italy.

He is currently a Full Professor of electronics with the University of Modena and Reggio Emilia, Modena and Reggio Emilia, Italy. He has authored and coauthored many technical and invited papers. His research interests include the characterization and modeling of Flash memory cells, the development of new nonvolatile cells, and the development of safety-critical and wireless applications for automotive electronics.

Dr. Pavan was in the Technical Committee of the International Electron Devices Meeting, the European Symposium on Reliability of Electron Devices, Failure Physics and Analysis, the International Symposium on VLSI Technology, Systems and Application, the International Reliability Physics Symposium, and the European Solid-State Device Research Conference. He was also a Guest Editor of the IEEE TRANSACTIONS ON DEVICE AND MATERIALS RELIABILITY.